

# **FLOW AND COMPACTION DURING THE VACUUM ASSISTED RESIN TRANSFER MOLDING PROCESS<sup>1</sup>**

Brian W. Grimsley<sup>†</sup>, Pascal Hubert<sup>††</sup>, Xiaolan Song<sup>†††</sup>,  
Roberto J. Cano<sup>†</sup>, Alfred C. Loos<sup>†††</sup>, R. Byron Pipes<sup>††</sup>

<sup>†</sup> NASA Langley Research Center, Hampton, Virginia 23681

<sup>††</sup> Old Dominion University, Norfolk, Virginia 23508

<sup>†††</sup> Virginia Polytechnic Institute and State University, Blacksburg, Virginia 24061

## **ABSTRACT**

The flow of an epoxy resin and compaction behavior of carbon fiber preform during vacuum-assisted resin transfer molding (VARTM) infiltration was measured using an instrumented tool. Composite panels were fabricated by the VARTM process using SAERTEX<sup>®2</sup> multi-axial non-crimp carbon fiber fabric and the A.T.A.R.D. SI-ZG-5A epoxy resin. Resin pressure and preform thickness variation was measured during infiltration. The effects of the resin on the compaction behavior of the preform were measured. The local preform compaction during the infiltration is a combination of wetting and spring-back deformations. Flow front position computed by the 3DINFIL model was compared with the experimental data.

KEY WORDS: Composites, VARTM, Process Modeling

## **1.0 INTRODUCTION**

Vacuum-assisted resin transfer molding (VARTM) is a variant of the traditional resin transfer molding (RTM) process. It has been developed over the last ten years for application in both commercial and military, ground-based and marine composite structures [1-3]. The process has advantages over conventional RTM by eliminating the costs associated with matched-metal tooling, reducing volatiles emission, and allowing low injection pressures [4]. VARTM is typically a three-step process including lay-up of a fiber preform, impregnation of the preform with resin, and cure of the impregnated preform. The reinforcement, in the form of woven carbon or glass fabric, is laid onto a rigid tool surface. The matched metal tool commonly found in RTM is replaced in the VARTM process by a formable vacuum bag material. The resin is injected through single or multiple inlet ports depending upon part size and shape. A vacuum

---

<sup>1</sup> This paper is declared a work of the U.S. Government and is not subject to copyright protection in the United States.

<sup>2</sup> Use of trade names or manufacturers does not constitute an official endorsement, either expressed or implied, by the National Aeronautics and Space Administration.

port allows the fiber preform to be evacuated prior to injection and provides the mechanism for transfer of the resin into the part. In addition to the pressure gradient caused by the vacuum pressure, gravity and capillary flow effects must also be considered [5]. The preform infiltration time is a function of the resin viscosity, the preform permeability and the applied pressure gradient. The infiltration time can be greatly reduced by utilizing a distribution medium with a higher permeability than the preform [6,7]. Consequently, the resin flows in the distribution medium first and then the infiltration process continues through the preform thickness.

In the present work, a detailed analysis of the VARTM infiltration process is presented. An instrumented VARTM system was designed to measure resin pressure and panel displacement at different locations in the panel during the infiltration process. The flow front position on the bag side and tool side of the panel is also measured. The panel quality was evaluated by analyzing panel void content and fiber volume fraction measurements. The observed preform deformation behavior during infiltration was compared to the preform compaction curves measured in quasi-static compaction. Finally, the relation between panel consolidation and resin pressure and the potential impact on the maximum achievable fiber volume fraction is discussed.

**1.1 Resin Flow** Complete filling of the mold with adequate wetting of the fibrous preform is the primary objective in VARTM. Incomplete impregnation in the mold leads to the production of defective parts with dry spots. Therefore, simulation of a resin flow through the preform is an important step in modeling the manufacturing process. Flow of resin through fibrous media can be modeled using Darcy's law [5]. The finite element/control volume (FE/CV) method is commonly used to model the resin flow through the preform. In this approach, the preform and distribution medium are first discretized into finite elements. A control volume is constructed around each node by subdividing the elements into smaller volumes. The pressure distribution in the resin filled region is obtained by use of the finite element method and Darcy's law is applied to calculate the flow rates. The concept of control volume and fill factors is then employed to track the location of the flow front [8]. Sun et al. [9] investigated mold filling for the Seeman's Composites resin infusion molding process (SCRIMP) using a high-permeable medium to infiltrate the preform. The authors found that the distribution medium can significantly reduce infiltration time. The simulation results also indicated that the infiltration time was a strong function of the permeability of the distribution medium, but was not sensitive to the preform permeability [9].

Hammani [10] studied the effects of the primary processing variables in the vacuum infusion molding process and presented a 1-D model for the process. The parameters investigated were the compaction of the reinforcement, the permeability, the infusion strategy and the presence of flow enhancement medium. The vacuum infusion molding process differs from the traditional RTM process because the flexible nature of the vacuum bag is coupled to the varying pressure inside the mold cavity. This results in a variation of the cavity thickness during the vacuum infusion impregnation process. In addition to the governing equations deriving the flow model, i.e., Darcy's law and the continuity equation, a new equation was introduced to account for the transverse pressure equilibrium inside the mold cavity during impregnation. Taking into account that the mold cavity thickness is pressure dependent and the permeability is a function of the fiber mat thickness, the theoretical model produced results in good agreement with the infusion

experiment. This approach was also used in the SCRIMP infiltration model developed by Han et al. [11].

**2.1 Preform Compaction** Few studies have been found in the literature regarding compression behavior of the reinforcement during VARTM, i.e., under low compaction pressure ( $\leq 1$  atm). Hammami [12] conducted compaction tests with the maximum compaction pressure not exceeding 1 atm. The compaction behavior of various preform and distribution medium architectures was investigated. It was found that the presence of the distribution medium significantly affected the compaction of the preform. Also, different compaction curves were observed for dry and wet conditions. Robitaille and Gauvin [14] studied the reorganization of the fiber network and the effect of friction. The results of sequences of successive compaction cycles applied to dry preforms and to preforms saturated in distilled water and silicon oil were presented. It was shown that the major reorganization mechanism during the first compaction cycle was lateral spreading of the rovings. It resulted in a significant rise of maximum fiber volume fraction. As the fiber volume fraction continued to rise, the compaction behavior became essentially dependent on the frictional characteristics of the fiber contacts. Chen et al. [15,16] developed a micromechanical model to study single-layer and multi-layer elastic deformation during the compaction of woven-fabric preforms in liquid composite molding processes. A 3-D model of the unit cell was proposed with certain assumptions. Based on this model and beam theory, analytical expressions for relationships between the fiber volume fraction, the applied compressive force, and preform thickness reduction were established. Loos et al. [17] performed experiments to obtain the relation between the fiber volume fraction and the state of stress in the dry preform. The experimental data of the fiber volume fraction were fit as a fourth order polynomial function of the compaction pressure.

## 2.0 EXPERIMENTAL

**2.1 Infiltration Experiments** An aluminum tool 1.27 cm in thickness was instrumented to allow for measurement of pressure and displacement of the preform during the VARTM infiltration. As shown in Figure 1, the pressure sensors (Omega Engineering, Inc., Series PX102) labeled P1 through P3 were mounted at the tool surface beneath the fiber preform. Linear Variable Displacement Transducers (LVDT, Omega Engineering, Inc., Series 400) labeled T1 through T3 were supported above the vacuum-bagged preform by a rigid beam. Sensors were recorded by a PC-based data acquisition system using LabVIEW<sup>®</sup> software. The flow front at the vacuum bag surface of the part was recorded using a digital video camera.

Composite panels (60 cm by 30 cm) were fabricated by the VARTM process using SAERTEX<sup>®</sup> multi-axial, non-crimp carbon fiber fabric and the A.T.A.R.D. SI-ZG-5A epoxy resin. Panel 1 contained one stack of fabric of ply sequence, [45,-45,0,90,0,-45,45], while Panel 2 and Panel 3 contained four stacks [45,-45,0,90,0,-45,45]<sub>2S</sub>. For Panel 1, 300 grams each of part A and B SI-ZG-5A epoxy were mixed by hand stirring. In Panel 2, 800 grams each were mixed. For Panel 3, the mixed resin was aged at room temperature for 30 hours. The resin viscosity was measured using a Rheometrics ARES System 3 parallel-plate rheometer. The resin viscosity was determined to be 0.27 Pa·s for Panels 1 and 2 and 0.60 Pa·s for Panel 3. The mixed resin was degassed at room temperature under full vacuum for approximately one hour.

The preform was cut and placed on the tool so that the 0° rovings were length-wise, or parallel to the direction of resin flow. A layer of Armalon fabric was placed above the preform to serve as a release layer. The distribution medium, containing three layers of nylon mesh screen, was laid on top of the preform and release layer. The medium was cut to dimensions of 60 cm by 27.4 cm allowing a 1.3 cm gap between the edge of the medium and the edge of the preform along the length. The distribution medium was terminated at a distance 2.5 cm from the end of the preform. These gaps prevented race-tracking of the resin as it flowed through the medium and the fiber preform. A 5.0 cm portion of the media was extended beyond the panel at the inlet side for inlet tube placement. Spiral-wrap tubing was stretched across the width of the panel on top of this section of medium to provide an even supply of resin to the part. A 0.95 cm inside diameter reinforced-vinyl tube was used to supply resin to the part. Both the vinyl and spiral tubing were also connected on the vacuum side of the part. The outlet tubing was connected to a resin trap and vacuum pump. The bagging procedure was completed when the preform, medium and tubing were sealed to the aluminum tool using a conformable vacuum bag and sealant tape.

The sealed bag and tubing were first evacuated to 97 kPa (1 in Hg) in order to zero the LVDT's and check for leaks using the pressure sensors. The vacuum pressure was then increased slowly to full vacuum and held there until the measured displacement reached equilibrium. The free end of the inlet tube was placed in the pot containing the degassed resin. A tube clamp was opened to allow the resin to flow into the spiral tubing, through the distribution medium and into the fiber preform, as shown in [Figure 2](#). When the preform was fully impregnated, as confirmed through visual inspection, the inlet and then the outlet tube were closed. The part was then placed in an oven to cure. The cure cycle utilized for the panels consisted of a ramp from room temperature to 67°C at 1.1°C/minute and hold for 2.75 hours, followed by a ramp at 1.4°C/minute to 123°C and hold for 2.75 hours. The part was then cooled at 1.0°C/minute to room temperature, released from the tool, rebagged, and postcured under full vacuum for six hours at 177°C. For this cure cycle, the gel point of the epoxy was reached at 180 minutes into the cycle [18].

**2.2 Preform Compaction Experiments** Experiments were conducted to develop an understanding of the response of the SAERTEX<sup>®</sup> fabric at the low pressure experienced during VARTM processing. The instrumented tool plate described earlier was used to measure the pressure and preform displacement. Four stacks of 15 cm x 15 cm fabric were placed on the tool surface between pressure sensors P1 and P2. For the dry preform tests, bagged preform was evacuated via one port located approximately 12 cm from the preform. In the wet compaction test, the bagging procedure was identical to that discussed in the Section 2.1 except that the distribution medium was not placed on top of the preform. An LVDT was placed above the center of the bagged part to monitor preform deformation. The bag was initially evacuated to 97 kPa to zero the LVDT. For the dry preform test, the bag pressure was slowly evacuated to full vacuum. Once the preform displacement stabilized, the bag was slowly vented to the atmospheric pressure. For the wet preform test, the preform was initially impregnated with SI-ZG-5A resin by applying a small pressure gradient to the preform (i.e. P1 = 1 atm and P2 = 0.9 atm). Once the preform was fully impregnated, full vacuum was applied to the bag until a steady state compaction deformation was measured. Then, the bag was slowly vented by opening the inlet and allowing resin to flow back into the preform.

Figure 3 shows the compaction tests results for the dry and wet preform. The curves shown correspond to the unloading portion of the test when the bag was vented to the atmospheric pressure. This essentially simulates the actual VARTM process but in a quasi-static condition. From Figure 3, the maximum achievable fiber volume fraction under full vacuum was 53% and 58% for the dry and wet preform, respectively. These results illustrate the significant lubrication effect of the wetting fluid on the compaction behavior of the preform reported by other authors [e.g. 12,13].

**2.3 Infiltration Experiment Results** Figure 4 shows a micrograph of the cross section of Panel 1. The figure shows that the fibers are well wetted by the resin and that the panel is essentially void free. Micrographs of sections for Panels 2 and 3 showed similar results. The fiber volume fraction of the panels, obtained by the acid digestion technique (ASTM D3171-76 [19]) was measured at different locations and average values of 45.5% ( $\pm 2.3\%$ ) and 49.7% ( $\pm 0.2\%$ ) were found for Panels 1 (one-stack) and 2 (four-stacks), respectively.

**2.3.1 Flow Front** Figure 5 shows the measured infiltration time with corresponding bag side and tool side flow front position. The bag side flow front position was directly obtained by image analysis of the video recorded during infiltration. The tool side flow front position was obtained from the tool pressure sensors response recorded during the test. Typically, the presence of the flow front at the tool surface is indicated by an increase in the pressure measured by the sensor. The flow front on the bag side surface reached the end of the distribution medium at 104, 148 and 270 seconds for Panels 1, 2 and 3, respectively. Figure 5 also shows the lag observed between the bag side and tool side flow front. The maximum lag measured was 19, 78 and 186 seconds for Panels 1, 2 and 3 respectively. In all cases, the bag side flow front slows significantly beyond the end of the distribution medium. The preform infiltration time was difficult to measure accurately. Nevertheless, the estimated preform infiltration time was 134, 239 and 510 seconds for Panel 1, 2 and 3, respectively. As expected, the increase in infiltration time and lag between the bag side and tool side flow fronts observed between Panels 1 and 2 is attributed to the increase in the preform thickness. For a given distribution medium dimension, an increase in preform thickness was shown to increase the transverse flow infiltration time and consequently the in-plane flow of the resin in the distribution medium. Furthermore, as shown from Panels 2 and 3, an increase of resin viscosity will also significantly increased the infiltration time and lag between the bag side and tool side flow fronts. In this particular case, a 0.33 Pa·s increase in resin viscosity resulted in a 113% increase in total infiltration time and 138% increase in the lag between the top and bottom flow front.

**2.3.1 Resin Pressure and Panel Thickness** Figures 6 and 7 present the infiltration data for Panels 1 and 2. The initial thickness corresponded to the preform thickness after the debulking step where the dry preform maximum packing is reached at a pressure of  $\approx 0$  kPa as measured by all the pressure sensors. As the resin flowed into the preform, the following observations were made:

- 1) The pressure sensors reacted as they came into contact with the resin. Then, the resin pressure rapidly increased to atmospheric pressure ( $\approx 101$  kPa). At all times, a resin pressure gradient existed in the flow direction (i.e.  $P_1 > P_2 > P_3$ ). For a thin panel (Panel 1), the pressure increase occurred more quickly compared to the thick panel (Panel 2).

- 2) For both panels, the average preform thickness was greater at the end of the infiltration process. In all cases,  $T1 > T2 > T3$  at the end, which indicates that the panel is less compacted on the resin inlet side and more compacted on the vacuum side.
- 3) For the thin panel,  $T1$  immediately increased at time,  $(t)$ ,  $t=0$  seconds (when the resin reaches the beginning of the preform), while  $T2$  decreased at  $t=49$  seconds. Then  $T1$ ,  $T2$  and  $T3$  increased more rapidly after 107 seconds. For the thick panel, the local thickness typically decreased first to a minimum value. The minimum thickness was reached at 22, 122 and 212 seconds for  $T1$ ,  $T2$  and  $T3$ , respectively. After the minimum thickness was reached,  $T1$ ,  $T2$  and  $T3$  increased in a manner similar to the thin panel.

The sudden increase in preform thickness observed at 107 seconds for Panel 1 (see [Figure 6](#)) corresponds to a sharp increase in resin pressure recorded by the pressure sensors. At the same time, the flow front reached the end of the distribution medium. The resistance to resin flow suddenly increased, causing the measured increase in pressure and panel thickness. This phenomenon was not as noticeable for the thick panel.

[Figure 8](#) shows the thickness ( $T2$ ) and corresponding pressure ( $P2$ ) measured at the center of the preform for Panel 3 (four-stacks and higher viscosity). In this figure, the different phases of the impregnation process can be isolated. From 0 to 90 seconds, the preform is dry and the measured pressure is constant at  $\approx 6$  kPa (full vacuum). After 90 seconds, the flow front reached the panel area under  $T2$  and the thickness began to decrease. From 90 to 300 seconds, the preform was impregnated by the resin from the top to the bottom of the preform (transverse flow). This is the wetting phase. The tool pressure sensor ( $P2$ ) began to react at 170 seconds, which indicates that the resin has reached the tool surface and that the fiber preform is fully saturated with resin. After 300 seconds, the wet preform (fully saturated) began to spring-back as indicated by the increase in the measured thickness. As shown in [Figure 8](#), this spring-back phenomenon corresponded to an increase of resin pressure toward atmospheric pressure ( $\approx 101$  kPa).

### 3.0 DISCUSSION

The compaction and infiltration experiments presented above revealed a number of important phenomena present in the VARTM process. It is well accepted that during flow of resin in fiber preforms, the total external pressure applied to the composite is equal to the sum of the resin pressure and the pressure supported by the fiber network [11]. For the VARTM process, the external pressure applied is the atmospheric pressure ( $P_{ATM}$ ):

$$P_{ATM} = P_R + P_F \quad (1)$$

where  $P_R$  is the resin pressure and  $P_F$  is the fiber pressure (pressure supported by the preform). The fiber pressure is primarily a function of the preform fiber volume fraction, but is also strongly influenced by the presence of a wetting fluid as shown in [Figure 3](#). On the other hand, the resin pressure is influenced by the boundary conditions applied at the flow front and at the



resin supply. For a standard VARTM process, the resin pressure is maintained at 1 atm in the injection reservoir and 0 atm at the flow front (vacuum side).

Figure 9 presents observed preform deformation and the different compaction mechanisms and their respective implication on the fiber and resin pressure. In the dry condition (Figure 9a) the preform essentially supports the external pressure,  $P_F = P_{ATM}$ , and a dry maximum debulking deformation of the preform is reached. During infiltration, two deformation mechanisms are present in the wet area of the preform: the wetting compaction and the spring-back. The wetting compaction (Figure 9b) is caused by a change of the arrangement or state of the fiber network, which is created by the lubrication effect of the wetting fluid. Under a given external pressure, the lubrication of the dry preform will cause an increase in the preform compaction ( $\epsilon$ ) by an additional amount of wetting deformation ( $\epsilon_w$ ). In VARTM, this phase typically takes place at high fiber pressure ( $P_F \approx P_{ATM}$ ) and low resin pressure ( $P_R \approx 0$ ). The preform spring-back mechanism (Figure 9c) occurs when the local resin pressure increases. According to Equation (1), the fiber pressure must decrease when the resin pressure increases. Consequently, the preform compaction ( $\epsilon$ ) decreases by an amount of spring-back deformation ( $\epsilon_s$ ) due to the reduced pressure carried by the preform. Figure 10 illustrates that the spring-back displacement observed during a VARTM infiltration corresponds to the unloading of the wet preform measured during the preform compaction test. It is clear that at any time during the infiltration process, the net compaction of the preform will depend on the relative magnitude of the wetting and the spring-back deformation mechanisms. These phenomena have also been observed by Williams, et al. [13] for different preform and resin systems. Under typical VARTM conditions, the spring-back deformation will dominate, as the resin pressure approaches atmospheric pressure toward the end of the infiltration process. Moreover, if a small leak is present in the bag, the bag pressure and consequently the resin pressure will reach the atmospheric pressure and the spring-back will be maximized. This may have happened in the current experiments since relatively low fiber volume fraction of the finished part were measured. In the present experiment, the wetting compaction was rapidly overcome by the spring-back for the thin panel (Panel 1). In thicker panels (Panels 2 and 3), the effect of the wetting compaction was observed before the spring-back began to dominate the infiltration process.

The incorporation of these deformation mechanisms in a comprehensive flow-compaction model allows for a more thorough investigation of the geometric, material and processing conditions that affect the observed compaction mechanisms in these experiments. Preliminary simulations using a three-dimensional model, 3DINFIL [5], were performed. This model simulates the VARTM process including capillary pressure and gravitational force effects. Figure 11 shows the results for the simulation of the infiltration of Panel 1 compared to the experimental data. The compaction of the preform presented in Figure 3 was incorporated in the model. Good agreement was found for the position of the flow front at the bag side and tool side of the preform.

## 4.0 CONCLUSIONS

The compaction behavior of the SAERTEX<sup>®</sup> multi-axial non-crimp carbon fiber fabric is very different in the dry and wet conditions. The maximum achievable fiber volume fraction under full vacuum was 53% and 58% for the dry and wet preform, respectively. Panel thickness and resin viscosity influenced the preform infiltration time. Infiltration time increased by 78% from

134 to 239 seconds when the preform thickness was increased from one to four stacks (400%). Increasing the resin viscosity by 122% from 0.27 to 0.60 Pa·s resulted in a total infiltration time increase from 239 to 510 seconds or 113%. During the infiltration process, the resin pressure in the preform rapidly increased to the atmospheric pressure. This resulted in an increase in preform thickness, which led to a reduced panel fiber volume fraction ranging from 45.5% to 49.7%. The compaction at the flow front was shown to be a complex combination of wetting deformation caused by resin lubrication and of spring-back deformation caused by the increasing resin pressure and corresponding decreasing preform pressure. The present results showed agreement with observations by Williams et al. for the resin infusion under flexible tooling (RIFT) process [13].

## 5.0 REFERENCES

1. S.M. Lewit and J.C. Jakubowski, SAMPE International Symposium, 42, 1173 (1997).
2. L.B. Nquyen, T. Juska and S.J. Mayes, AIAA/ASME/ASCE/AHS/ASC Structures, Structural Dynamics, and Materials Conference, 38, 992 (1997).
3. Lazarus, P., SAMPE International Symposium, 41, 1447 (1996).
4. J.R. Sayre, “RFI and SCRIMP Model Development and Verification”, Ph.D. Dissertation, Department of Engineering Science and Mechanics, Virginia Polytechnic Institute and State University, Blacksburg, VA (2000).
5. A.C. Loos, J.R. Sayre, R.D. McGrane and B.W. Grimsley, SAMPE International Symposium, 46, 1049 (2001).
6. Seemann, W.H., 1990. U.S. Patent 4,902,215.
7. Seemann, W.H., 1994. U.S. Patent 5,316,462.
8. H.P. Wang and H.S. Lee In C. L. Tucker, ed. Hanser Publishers, Fundamentals of Computer Modeling for Polymer Processing, Chapter 8, (1989).
9. X.D. Sun, S. Li and J.L. Lee, Polymer Composites, 19(6), 807-817 (1998).
10. A. Hammami and B.R. Gebart, Polymer Composites, 21(1), 28-40 (2000).
11. K. Han, S. Jiang, C. Zhang and B. Wang, Composites Part A, 31, 79-86 (2000).
12. A. Hammami, Polymer Composites, 22(1), 337-348 (2001)
13. D.C. Williams, M.S. Grove and J. Summerscales, Composites: Part A, 29(A), 111-114 (1998).
14. F. Robitaille and R. Gauvin, Polymer Composites, 20(1), 48-61 (1999).
15. B. Chen and T. Chou, Composites Science and Technology, 60, 2223-2231 (2000).
16. B. Chen, A.H. Cheng, and T.W. Chou, Composites: Part A, 32(A), 701-707 (2001).
17. A.C. Loos, B.C. Romesh, D. Ratazzi, A.C. Caba, and T. Knott, “Process Model Development / Residual Stress Model Development”, Final Report for the Boeing Company, Virginia Polytechnic Institute and State University, (1998).
18. B.W. Grimsley, P. Hubert, T.H. Hou, R.J. Cano, A.C. Loos, R.B. Pipes, The 16<sup>th</sup> Technical Conference on Composite Materials of the American Society for Composites, Blacksburg, VA, (2001) in press.
19. ASTM D3171-99, Annual Book of ASTM Standards, Vol. 15.03, American Society for Testing and Materials, Philadelphia, (2000).



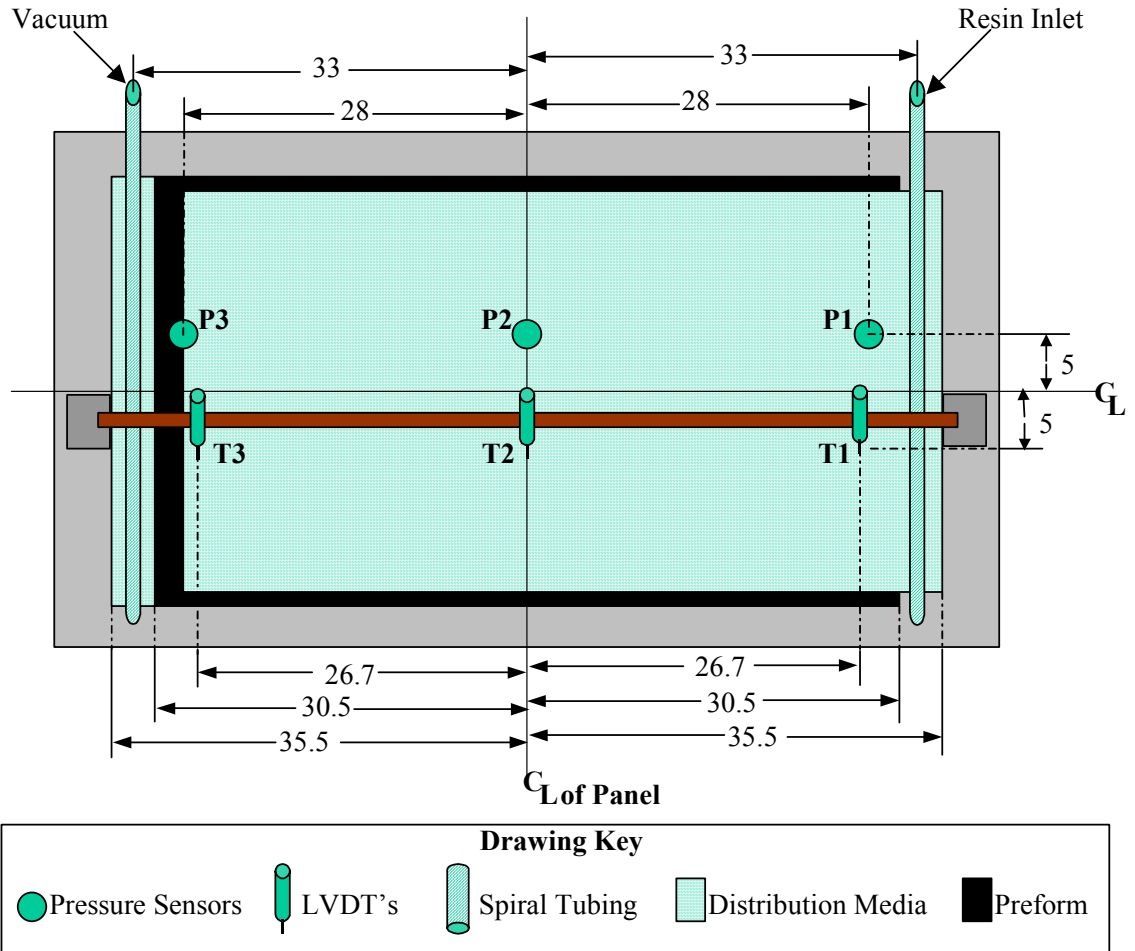


Figure 1. NASA Langley Research Center VARTM instrumented system (dimensions are in cm).

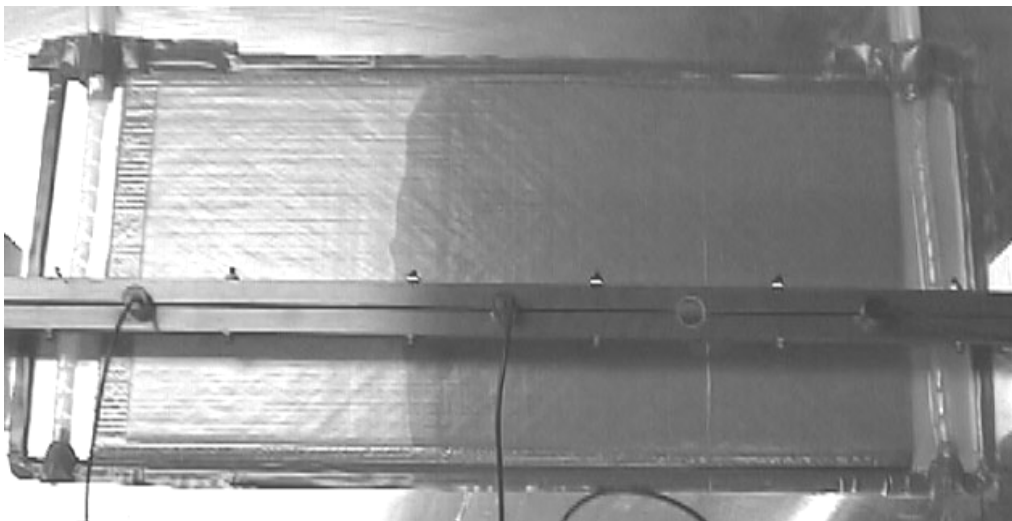


Figure 2. Photograph of a typical VARTM infiltration experiment.

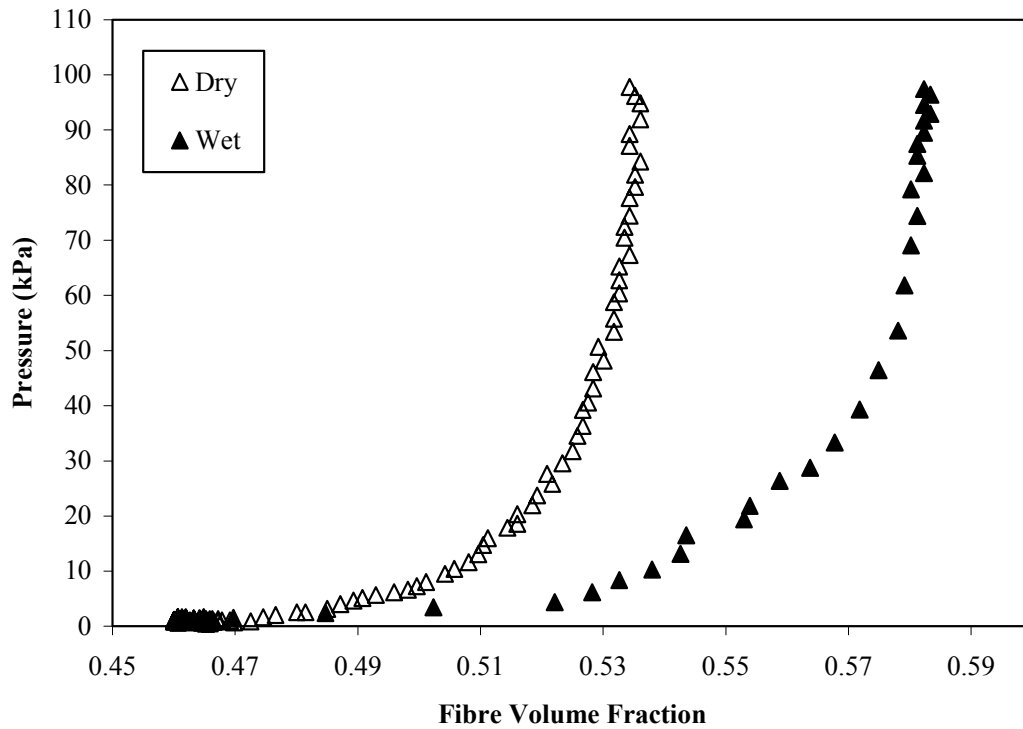


Figure 3. Compaction data for a  $[45,-45,0,90,0,-45,45]_{2s}$  of SAERTEX<sup>®</sup> multi-axial non-crimp carbon fiber preform in dry and wet conditions.

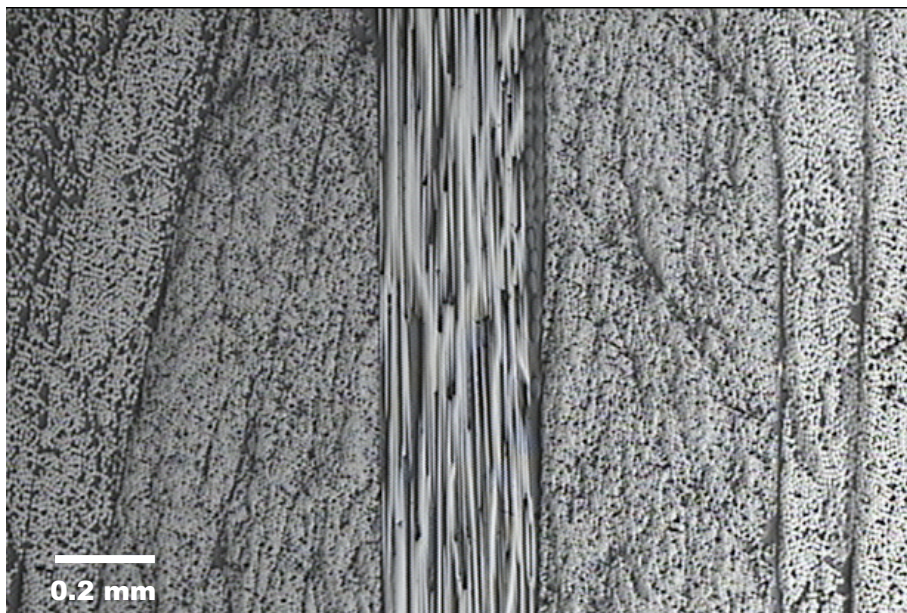


Figure 4. Cross-section micrograph of Panel 1 after cure.

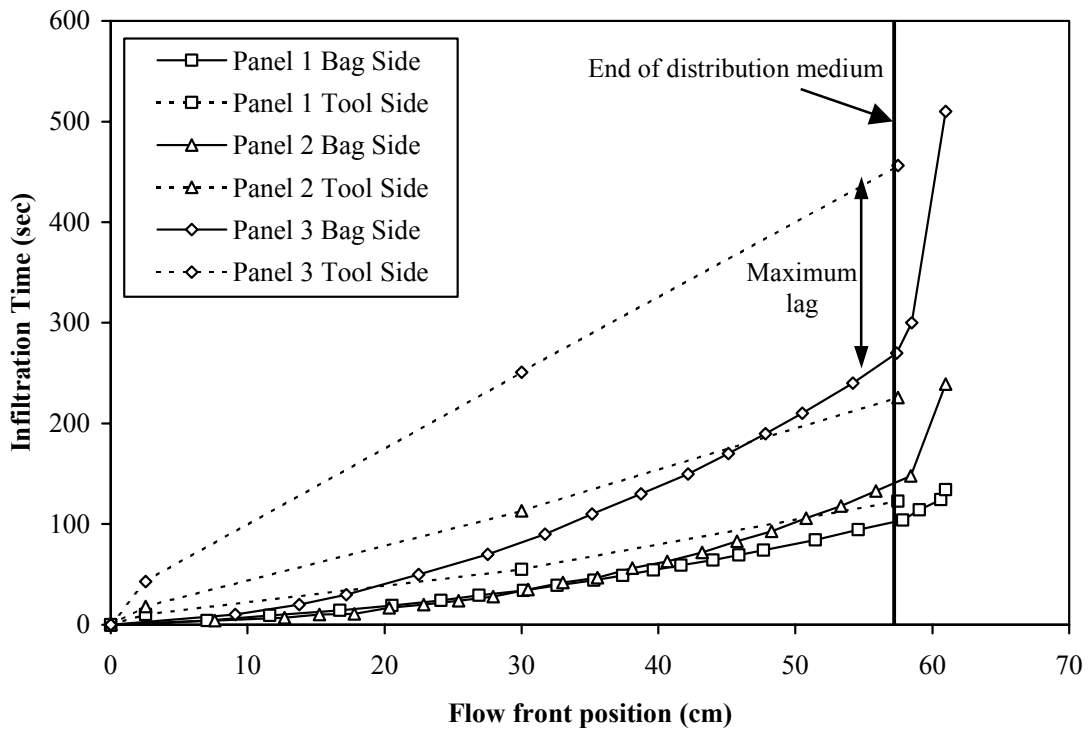


Figure 5. Infiltration times for bag side and tool side flow fronts.

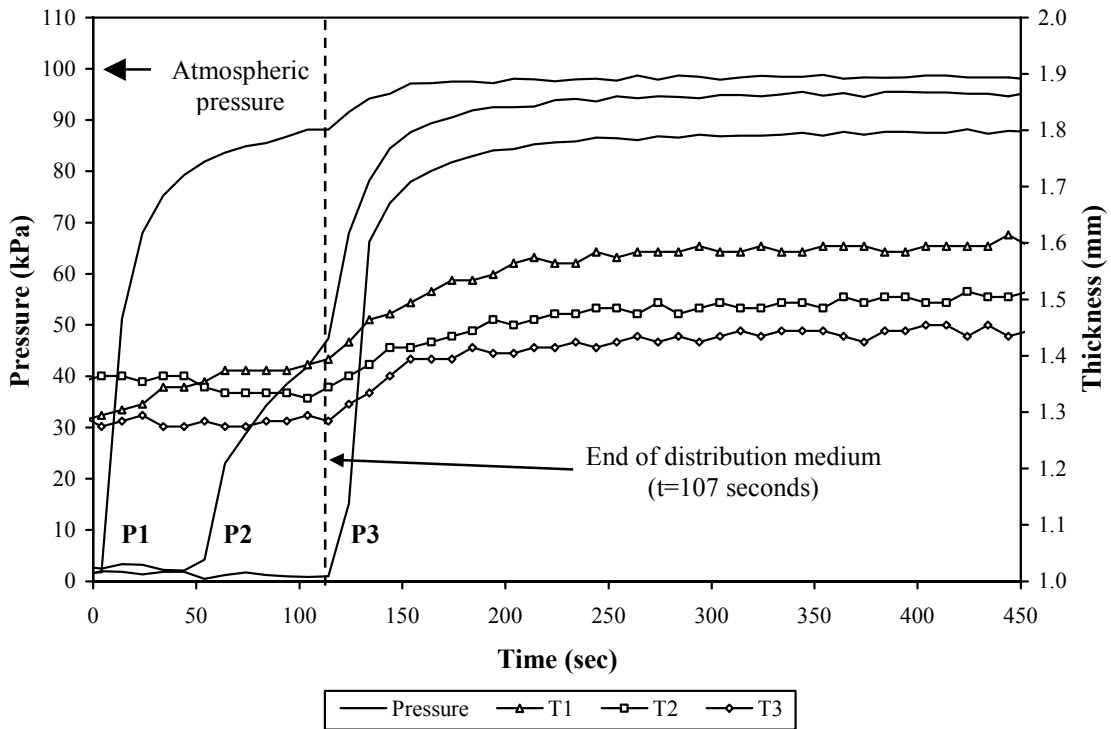


Figure 6. Infiltration data for Panel 1, SAERTEX<sup>®</sup> carbon fiber fabric (1 stack) and SI-ZG-5A epoxy resin.

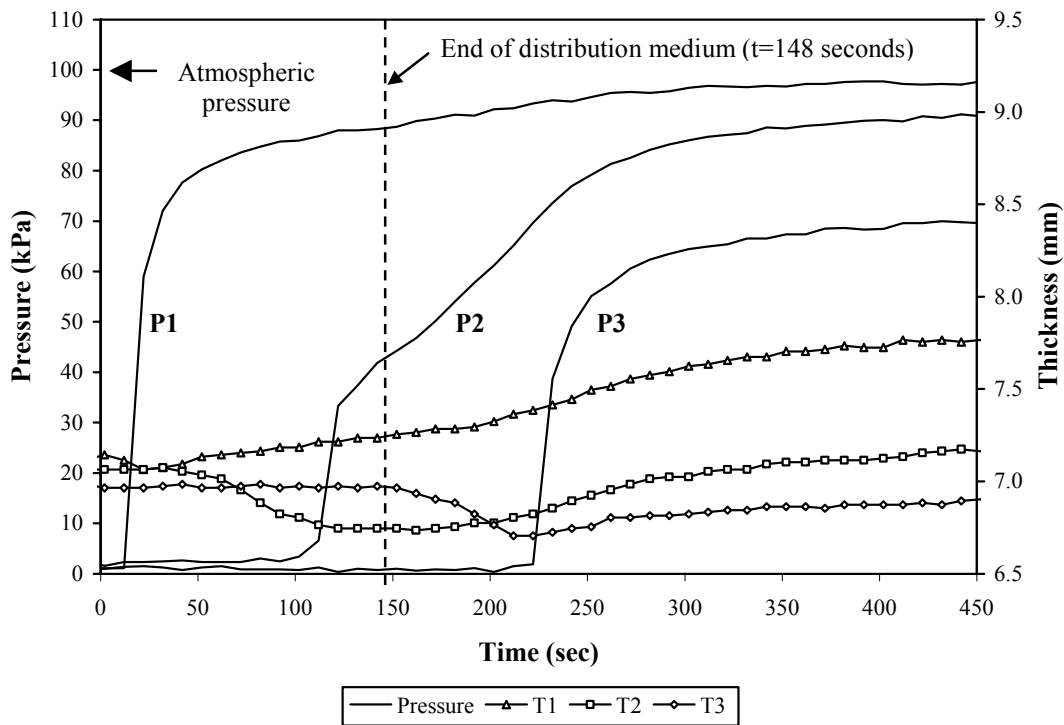


Figure 7. Infiltration data for Panel 2, SAERTEX<sup>®</sup> carbon fiber fabric (4 stacks) and SI-ZG-5A epoxy resin.

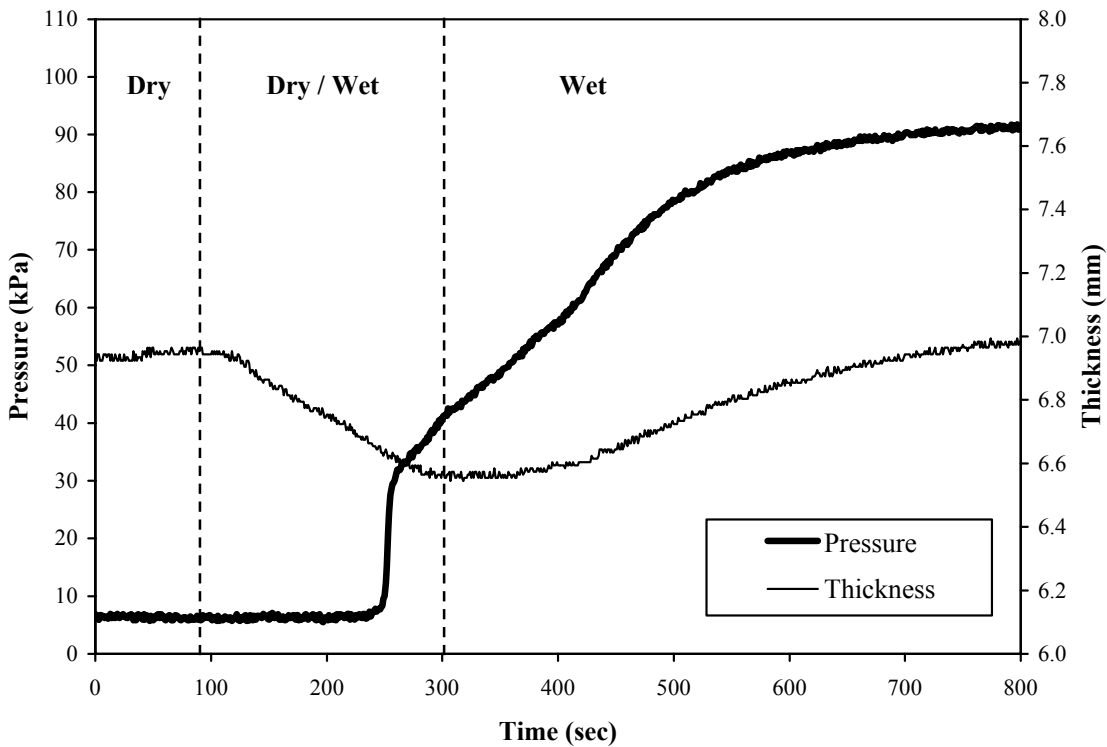


Figure 8. Pressure (P2) and panel thickness (T2) for Panel 3.

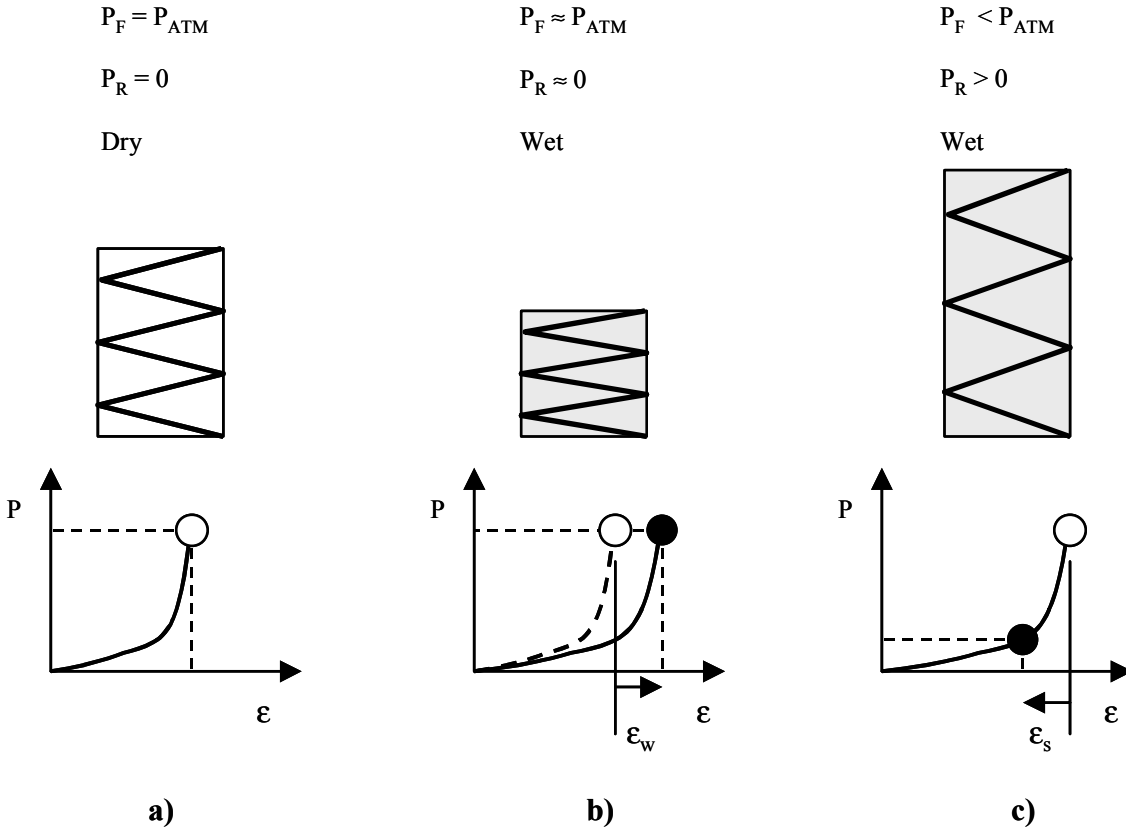


Figure 9. Compaction mechanisms during VARTM, a) dry compaction, b) wetting compaction and c) spring-back.

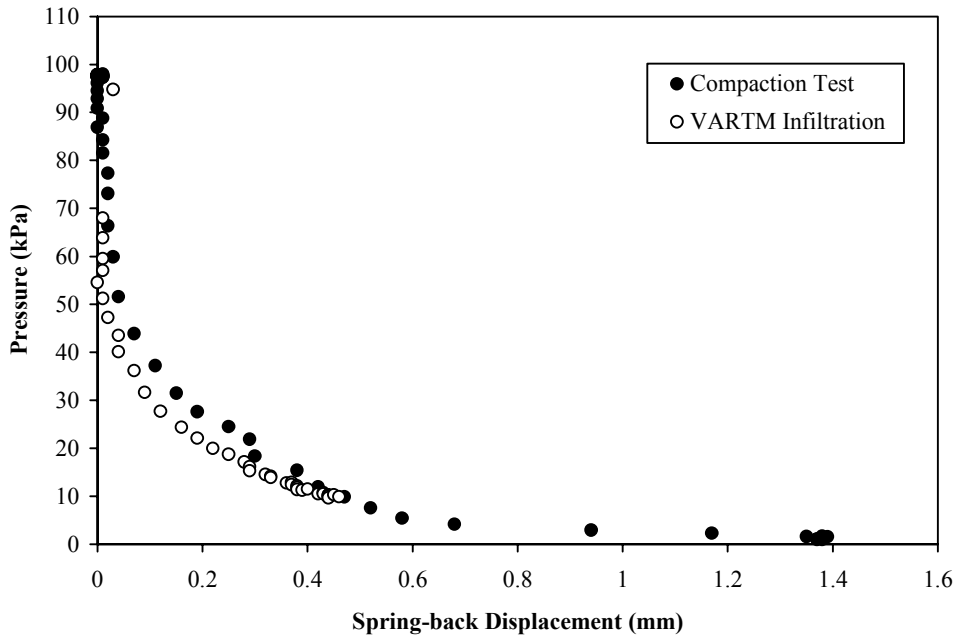


Figure 10. Spring-back displacement from compaction test and during VARTM infiltration (from T2 and P2 for Panel 2).

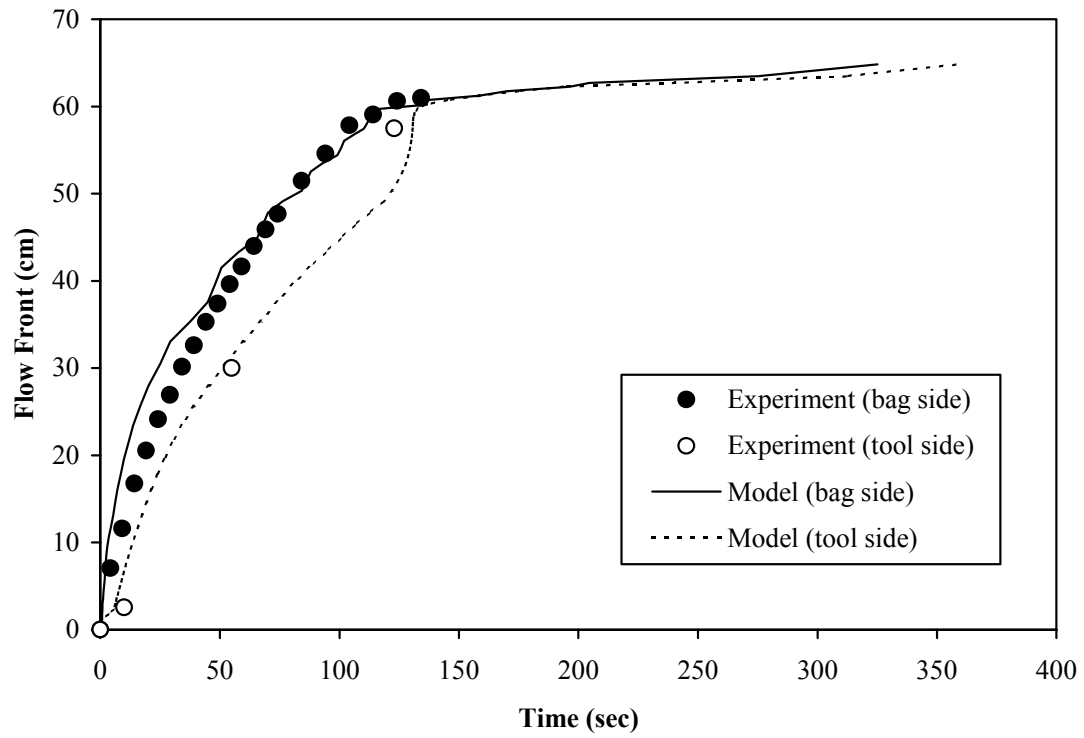


Figure 11. Flow front comparison between 3DINFIL simulation and experiment for Panel 1.